

X-RAY SPECTRA OF RECOIL IONS FROM FAST BEAM INTERACTION WITH Mg AND MgF₂ SOLID TARGETS

C.T. CHANTLER and J.D. SILVER

University of Oxford, Clarendon Laboratory, Parks Road, Oxford OX1 3PU, England

Magnesium multiple-vacancy Mg K α spectra and MgF₂ multiple-vacancy F K α spectra produced by fast ion bombardment of solid targets have been analysed with a 5'' curved crystal X-ray spectrometer. Transitions are observed in the region of the 1s²–1s2p helium-like transitions and their satellites. The dependence of the observed spectra on the angle of the target to the beam and the possibility of a precise measurement of wavelengths of highly-ionised recoils is discussed.

1. Introduction

Numerous studies [1–7] have been made of the spectroscopy of highly-ionized recoil atoms in gas targets. The low-velocity recoils produced in such experiments reduce Doppler shifts, enabling the precise measurement of the wavelengths of deexcitation from these excited states. Comparison to the theoretical wavelengths for hydrogenic and helium-like transitions has then served as a test of relativistic and quantum electrodynamical effects. Interest in the behaviour of such ions in laboratory and astrophysical plasmas [7–9] is also a motivating consideration.

In comparison to gas target spectroscopy, solid targets can yield high fluxes of highly charged particles as a consequence of the greater target densities. The use of a solid target enables high vacuum to be attained without the use of a cell or the extended sources from differential pumping. High precision gas recoil spectroscopy is generally restricted to the monatomic noble gases to avoid Coulombic explosion of the molecules involved. Conversely, solid target spectroscopy is potentially a more general technique and may also be used to investigate plasma–surface interactions.

Recently, interest in K α X-ray multiple-vacancy spectra has grown in relation to the effect of L-shell vacancy rearrangement upon satellite intensities [10–12]. Resonant electron -transfer from adjacent ions has been identified in gas and solid targets [13–15,5]. These and other effects have led to the desire for an accurate model for the intensity ratios of the transitions involved and to further observations of the lines at high resolution.

This paper reports the observation of multiple-vacancy Mg K α and F K α satellite and hypersatellite transitions using ions from a tandem Van de Graaff with varying angles of the target to the beam. Although other factors are involved, the results suggest a procedure for observing greater fluxes of highly-ionised atomic transitions, especially in the hypersatellite region.

2. Experiment

Well-collimated beams of 63MeV ³⁵Cl⁶⁺ and ³⁵Cl⁸⁺ ions from the Oxford 10 MV tandem Van de Graaff accelerator were directed onto solid targets of metallic magnesium and MgF₂. The targets were solid blocks 20 × 20 × 5 mm³ mounted on an aluminium support free to rotate. This was insulated from the beam line and used as a simple Faraday cup in the observations at 8° and 25° to the beam. At grazing incidence (3°) either this or the collection of the current incident on slits further downstream was used. Beam currents of 200 to 700 nA collected in this manner are relative and subject to secondary electron emission, but provide a consistent signal for optimisation and current normalisation during each scan.

The excited recoil emission was observed by a 5'' Rowland-circle curved crystal X-ray spectrometer mounted normal to the beam and 37.5° from the vertical. Adjustable entrance and detector slits collimated the emission into a flow proportional counter. Fluorine multiple-vacancies were observed using a RAP crystal with a resolution of $\lambda/\Delta\lambda \approx 240$, while magnesium ion emission was observed with an ADP crystal, giving spectral resolutions of ≈ 650 .

Spectra are collected using a programme modified from that of Klein et al. [3]. The spectrometer scans linearly with wavelength, and the spectra are calibrated by secondary sources. The fluorine spectra were calibrated using the known lines [3] from neon gas targets under identical conditions. Eight magnesium lines were used to calibrate the ADP crystal by correspondence to magnesium lines in lower resolution RAP

scans (not discussed here) and by the use of an X-ray source mounted on the solid target holder. The use of a stationary source of magnesium or aluminium (and tungsten) X-rays provided a confirmation of the wavelength calibration of the spectrometer.

3. Discussion: wavelengths

The five main spectra are shown in figs. 1–5. Relevant parameters for the spectra are given in table 1. The magnesium spectral lines are tabulated and compared in table 2. Relative intensities from the fitted areas under the peaks are given with the FWHM estimates. The Mg K α peak in the spectra was used as a calibration peak in order to provide consistent wavelengths independent of shifts resulting from variation of the spectrometer geometry between runs.

A small shift (0.008 Å) of the fitted position of the Mg K α line in the spectra with respect to the calibration was observed; this may be due to the excitation of M-shell electrons in the solid target emission. It is not due to the presence of *additional* electron density from adjacent ions in the solid. Only the statistical errors in the fitted wavelengths are given: errors due to the asymmetry of the peaks and to other shifts are neglected. In particular, there appears to be a shift between spectrum 1 and the other two of 0.005 Å for line 2, increasing to 0.016 Å for line 6. Changes in the

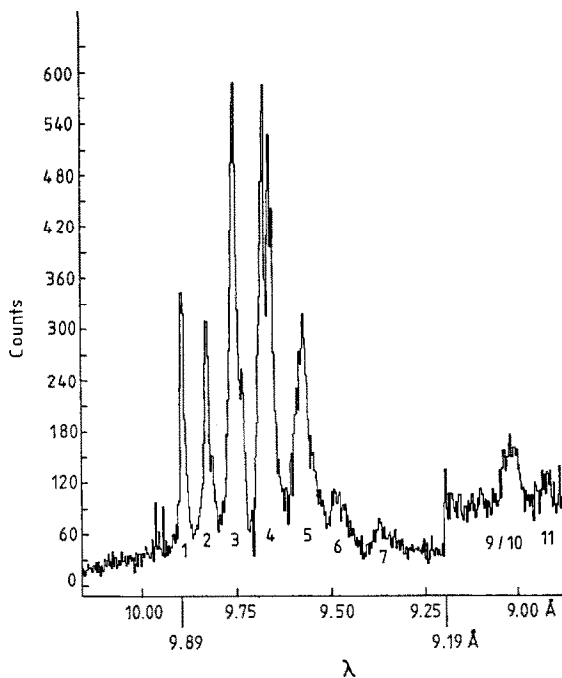


Fig. 2. Relatively short Mg spectrum from a solid target at 8° to the beam. The break at 9.19 Å (from a voltage change) enhances the signal by a factor of 3.

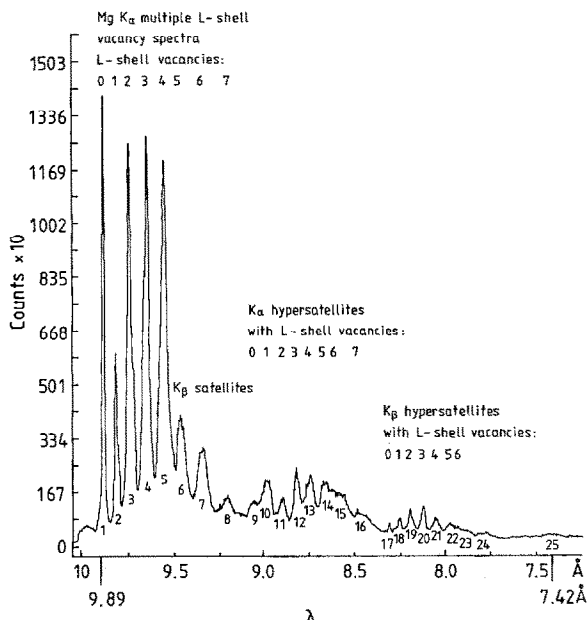


Fig. 1. Multiple-vacancy Mg K α spectrum with a Mg solid target at grazing incidence to the beam. Resolution circa 650.

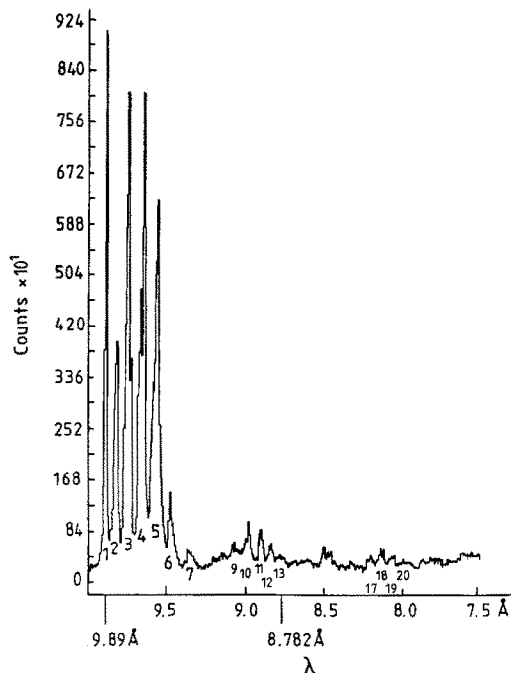


Fig. 3. Mg solid target spectrum taken with the target at 25° to the beam.

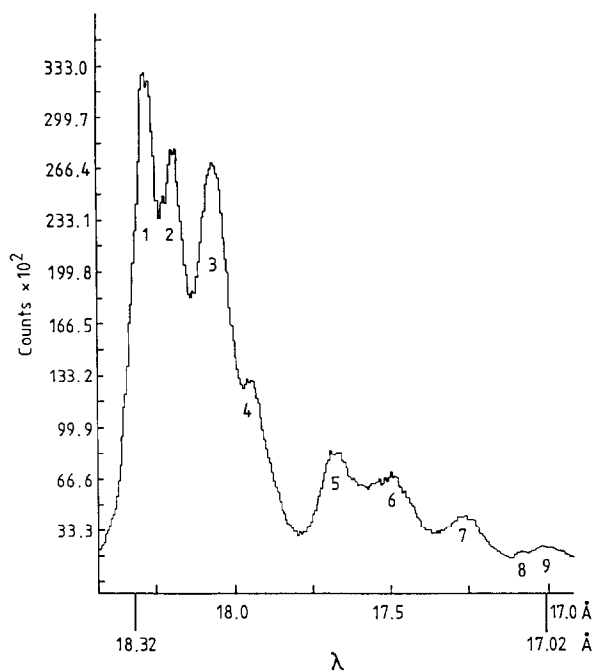


Fig. 4. Fluorine multiple-vacancy spectrum from a MgF_2 solid target at 3° to the beam (grazing incidence).

excitation and emission conditions could lead to greater M-shell recombination for the latter spectra, which would account for the variation, or they may be due to fitting errors.

The relation to well-known transitions and the identifications are given in the tables. Where lines are merged or attributed to the same multiple-vacancy charge state, the fitted components are denoted a, b, c with the major component capitalised. The identifications refer directly to the average-of-configuration energies calculated by Maurer and Watson [24] for various occupation numbers of M-shell electrons. These were calculated assuming a statistical and random population of the states. Closest correspondence is seen with the wavelengths of spectrum 1.

The line components should not be equated to corresponding configurations listed in the table; rather, they may be compared to the wavelengths for various config-

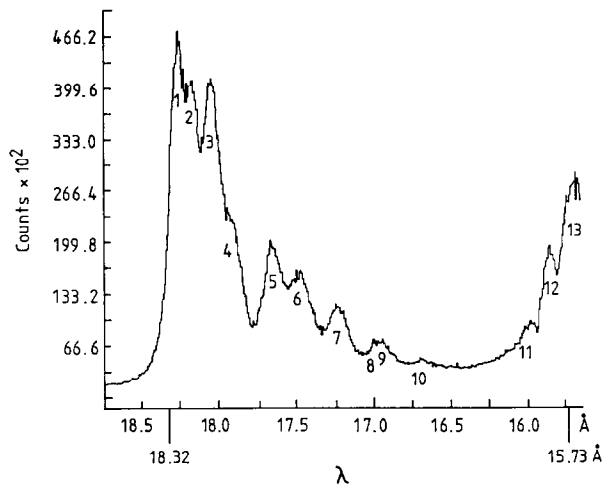


Fig. 5. Extended fluorine spectrum from MgF_2 at grazing incidence, showing hypersatellite peaks.

urations with different M-shell vacancies. For example, component 4a corresponds to $\text{Mg V (KL}^3)1s2p^33s^2-1s^22p^43s^2$ but 4B includes $1s2p^5-1s^22p^4$, $1s2s2p^43s-1s^22s2p^33s$ and $1s2s^22p^33s-1s^22s^22p^23s$ ($\text{Mg VII KL}^3\text{M}^2$ and $\text{Mg VI KL}^3\text{M}$) transitions.

The calculated wavelengths are averages over all terms in each configuration, so that although the $1s2s2p^4-1s^22s2p^3$ wavelength is given as 9.636 \AA , the $3P^-$ to $3S$ term yielded 9.745 \AA while the $3P^+$ to $3D$ term yielded 9.507 \AA [24].

The $K\beta$ line at 9.521 \AA [17] may be observed as an asymmetry between lines 5 and 6, while peak 8 is in the region of the helium-like $1s^2\ ^1S-1s2p\ ^1P, ^3P$ states (9.23 \AA and 9.168 \AA respectively). This confirms the calibration, as does the 8.470 \AA satellite to the $8.4177, 8.4230$ Lyman- α $1s-2p\ ^2P_{3/2,1/2}$ transitions [38] at peak 16.

Fluorine lines and identifications are given in table 3.

Few references have observed Mg or F multiple-vacancy spectra [10,11,13,14] and these [10,13] have concentrated on deriving intensity distributions rather than line positions and wavelengths. This is partly a consequence of the generally low resolution obtained and the low ionisation observed. The structure con-

Table 1
Selected parameters for the spectra

Spectrum	1	2	3	4	5
Beam	Cl^{6+}	Cl^{8+}	Cl^{8+}	Cl^{6+}	Cl^{6+}
Target	$\text{Mg}, 3^\circ$	$\text{Mg}, 8^\circ$	$\text{Mg}, 25^\circ$	$\text{MgF}_2, 3^\circ$	$\text{MgF}_2, 3^\circ$
Lines	Mg K	Mg K	Mg K	F K	F K
Region	$10.060-7.111 \text{ \AA}$	$10.166-8.874 \text{ \AA}$	$9.994-7.517 \text{ \AA}$	$18.781-15.636 \text{ \AA}$	$18.504-16.932 \text{ \AA}$

Table 2
Fitted wavelengths for magnesium lines

Lines:	Spectra			Calc: M-shell electrons		
	1	2	3	Ident. ^{b)}	3s ²	empty ^{c)}
1	9.8900 ^{a)} C(0.014)73	9.8900C(0.014)1.5	9.8900C(0.013)44	126–225	9.881	9.873
2A	9.8197 ± 2(0.015)34	9.8246 ± 8(0.016)1.4	9.8232 ± 1(0.021)27	125–224	9.821	9.809
2b	9.8026 ± 4(0.011)4.9	9.8080 ± 20(0.008)0.2		116–215	9.814	9.802
3a			9.7739 ± 5(0.015f)42 ^{b)}	115–214 ^{d)}	9.746	9.729
3B	9.7468 ± 2(0.023)106	9.7525 ± 5(0.022)4.1	9.7515 ± 2(0.023)62	124–223	9.740	9.722
3c	9.7224 ± 3(0.016)23	9.7292 ± 8(0.012)0.8	9.7278 ± 3(0.014)14.4	106–205	9.740	9.723
4a	9.6652 ± 5(0.022)53	9.6753 ± 11(0.021)3.2	9.6725 ± 6(0.016)26	105–204	9.666	9.644
4B	9.6460 ± 4(0.017)64	9.6534 ± 11(0.018)2.5	9.6541 ± 3(0.011)21.6	114–213	9.658	9.636
4c	9.6367 ± 90(0.029)20		9.6494 ± 36(0.022)22	123–222	9.657	9.635
5a		9.5868 ± 26(0.020f)0.6	9.5910 ± 7(0.020)14	104–203	9.571	9.543
5B	9.5539 ± 3(0.045)166	9.5665 ± 14(0.023)1.74	9.5656 ± 4(0.024)50	113–212	9.569	9.542
5c		9.5414 ± 26(0.020f)0.38	9.5443 ± 9(0.018)7	122–221	9.560	9.532
6	9.4604 ± 5(0.055)50	9.4760 ± 22(0.055)1.7	9.4756 ± 6(0.049)18	103–202	9.476	9.444
				112–211	9.465	9.434
				121–220	9.428	9.460
7	9.3415 ± 5(0.060)47	9.3647 ± 22(0.027)0.29	9.3525 ± 8(0.047)5.1	102–201	9.367	9.331
				111–210	9.362	9.325
8	9.2034 ± 11(0.050)9.8	not observed	not observed	101–200	9.259	9.218
9	9.0541 ± 14(0.052)11			Kα ² + KβL ⁴ ?		9.044
10	8.9845 ± 10(0.055)29	9.0129 ± 22(0.052)1.7	8.9836 ± 9(0.035)6	K ² L + KβL ³ ?		9.02–8.98
11	8.8971 ± 10(0.042)13	8.9255 ± 39(0.057)0.97	8.9042 ± 8(0.026)5.4	MgV ^{e)} K ² L ²		8.99–8.86
12	8.8194 ± 8(0.035)20		8.8441 ± 12(0.030)3.4	Mg VI K ² L ³		8.99–8.73
13	8.7498 ± 9(0.050)23		8.7815 ± 22(0.062)3.9	Mg VII K ² L ⁴		8.82–8.62
14	8.6669 ± 12(0.045)16		8.43–8.84 ^{b)}	Mg VIII K ² L ⁵		8.67–8.55
15	8.5967 ± 22(0.089)24		8.56–8.66 ^{b)}	Mg IX K ² L ⁶		8.54–8.48
16	8.4702 ± 7f(0.045)3		8.40–8.55 ^{b)}	Mg X K ² L ⁷		8.418
17	8.3082 ± 12(0.011)1			B1 ^{f)} Kβ ²		
18	8.2532 ± 12(0.020)3.1			B2 Kβ ² L		
19	8.1922 ± 12(0.027)6.5			B3		
20	8.1211 ± 12(0.025)7.4			B4		
21	8.0470 ± 14(0.030)4.3			B5		
22	7.9725 ± 23(0.025)1.5			B6		
23	7.9361 ± 84(0.084)4.2			B7		
24	7.7977 ± 31(0.102)6.3			B8 Kβ ² L ⁷		
25	7.4213 ± 55(0.084)2.2					
L-shell vacancy fraction		Kα satellites 3.03 Kβ K ² L ⁿ 3.86	Kα satellites 2.70	Kα satellites 2.48		

^{a)} The wavelengths, errors in the last digit(s) and fwhm in parentheses are in Å; the uncorrected fitted intensities are in units of 1000 counts (summed over channels). C: used for calibration.

^{b)} Identification–*ijk* represents the configuration 1sⁱ2s^j2p^k3sⁿ.

^{c)} Maurer and Watson [24]. These theoretical values have errors of ±0.02 Å.

^{d)} Line 3a is *not* 1s2s2p⁵–1s²2s2p⁴ – see the text for an explanation.

^{e)} Mg #: # – 1 vacancies; strictly all assignments should be K^aL^bMⁿX, where *n* = 0, 1 or 2 vacancies in the 3(s) shell and X may represent any satellites or excited levels. For example, line 16 could be Mg X K²L⁷ or Mg XI K²L⁷M or (nearly) Mg XII K²L⁷M².

^{f)} B*n*: the Kβ hypersatellites are labelled as B1–B*n*.

^{g)} Armour et al. [8].

^{h)} The f indicates that the parameter given was fixed in the analysis because the peak was faint and poorly resolved.

tained in spectrum 1 correlates with beam–foil limits and calculations for highly ionised transitions [8–9], represents a substantial improvement upon other multiple-vacancy MgK spectra and allows reasonable line positions to be derived. Notably, the ionization is greatly

enhanced and may best be compared with the sodium spectra of Watson et al. [15].

This enhancement can be attributed to the use of grazing incidence geometry, possible with the experimental method used. The major advantage of grazing

Table 3
Wavelengths and comparison for fluorine lines

Spectrum: Line	4 (MgF ₂ , Cl)	5 (MgF ₂ , Cl)	Identification	FI 18.295 ^{c)}
1	18.320 ± 4(0.107)516 ^{a)}	18.320 ± 4(0.132)880	FII Kα 18.32 ^{b)}	18.297–18.145 ^{c)}
2	18.222 ± 4(0.075)245	18.222 ± 4(0.075)256	FIII (and II)	18.260–17.868 ^{c)}
3	18.106 ± 4(0.120)478	18.109 ± 4(0.138)776	FIV (and III)	18.177–17.567 ^{c)}
4	17.971 ± 5(0.132)198	17.963 ± 5(0.132)296	FV (and IV, III) F K-edge	18.024–17.477 ^{c)} 17.913 ^{b)}
5	17.709 ± 4(0.120)121	17.707 ± 4(0.126)229	FV (and IV)	
6	17.537 ± 5(0.201)178	17.529 ± 4(0.176)253 FVI 1s2s ² 2p ³ P–1s ² 2s ² 1S 17.452 ^{e)} FVI 1s2s ² 2p ¹ P–1s ² 2s ² 1S 17.324 ^{e)} FVII 1s2p ² 4P–1s ² 2p ² P 17.318 ^{e)}	FVI (and V)	17.700–17.127 ^{c)} 17.473 ^{c)} 17.341 ^{c)} 17.324 ^{c)}
7	17.285 ± 4(0.138)65	17.284 ± 4(0.126)119	FVII (and VI)	17.362–16.949 ^{c)}
8	17.107 ± 5(0.027)1.2		FVIII 1s2s ³ S–1s ²	17.15 ^{b)}
9	17.018 ± 7(0.138)26	17.000 ± 4(0.126)47	FVIII 1s2p ³ P–1s ²	16.950 ^{d)} 16.968 ^{c)}
10		16.732 ± 18(0.065)6.8	FVIII 1s2p ¹ P–1s ² FII K ² L ⁻¹ FIII K ²	16.806 ^{d)} 16.818 ^{c)} 16.279 ^{c)} 16.303–16.156 ^{c)}
11		16.033 ± 39(0.239)30	FIV K ² L	16.258–15.946 ^{c)}
12		15.897 ± 4(0.063)99	FV K ² L ²	16.158–15.656 ^{c)}
13		15.730 ± 6 (0.170)485	FVI K ² L ³ 2s2p ³ FVII K ² L ⁴ 2s2p ²	15.812–15.422 ^{c)} 15.570–15.272 ^{c)}
L shell vacancy fraction Kα satellites 2.04 Kα satellites 2.07				

^{a)} Wavelengths and fwhm are in Å; statistical errors are in the last significant digits; areas are in 1000 counts (summed over channels).

^{b)} Helium-like wavelengths are obtained from ref. [16]. Kα, β from ref. [17] are used. Assignations are discussed in the text.

^{c)} Values from ref. [24].

^{d)} Values from ref. [18].

^{e)} Values from ref. [9].

incidence lies in relation to absorption effects in the solid target. This is clear in the contrast between spectra 1 and 3. The former has strong Kα and Kβ hypersatellites and high vacancy satellite lines whereas the lines above the K edge in spectrum 3 (line 5c) are greatly reduced in intensity. The greater angle focuses the beam onto a smaller region of the target, allowing greater count rates at the detector after the collimation of the slits. However, more of the excitation occurs in deep layers, so that any transitions above the strong absorption edge are strongly reabsorbed before leaving the solid. Some of this energy may be reradiated as Kα single-vacancy spectra after electron transfer and deexcitation. This has been seen in other work and is evident in spectra 2 and 3.

The fluorine spectra show the Kα satellite and hypersatellite lines. Assuming that the fluorine line distribution follows that of magnesium, the peak ionization state may be seen to be the F IV KL² peak. The resolution is insufficient to identify any satellite structure around each peak, but the presence of M-shell excitations [19] is assumed even though the ground state contains no M-shell electrons.

The most impressive result of the fluorine calibration is the group of satellites to the helium-like peaks separated from surrounding structure. Line 8 may be a satellite to the ³P transition rather than the 1s2s³S proposed. These lines involve the excitation or ionization of nearly all strongly-bound (K and L-shell) electrons. With fluorine, the only electrons in higher orbitals will be those excited but not ionized by the interaction and those relaxing into outer shells before radiative deexcitation. This is unlikely to involve more than a few electrons since the inelastic energies imparted to the electrons are sufficient to provide a significant outward velocity. It is also reasonable to expect most electrons in higher shells of magnesium to be ionized or only weakly interacting with the recoil ion. It is therefore likely that solid targets may be used for few-electron wavelength studies at higher resolution.

4. Intensities: simple estimates

Tables 2 and 3 provide the fitted intensities from least-squares analysis uncorrected for background, ab-

sorption, overlap and other effects. These intensities may be used to provide crude estimates of L-vacancy production and electron recombination and of the effect of absorption.

From fig. 1 the magnesium $K\alpha$ and $K\beta$ satellites and hypersatellites all exhibit the same intensity distribution. The base MgI $K\alpha$ (L-K) line is enhanced from nonradiative decay processes while the apparent ionization distribution peaks at the fourth vacancy (the third L-shell vacancy) both in the satellite and hypersatellite intensities.

This is not reflected in the fitted intensity of line 5 due to the addition of a $K\beta$ tail. The ratio of $K\beta$ to $K\alpha$ intensities is much greater than expected from tabulated values and light ion impact, which would predict $K\beta/K\alpha \approx 0.02$ [29,32]. This is probably due to selective electron capture from adjacent orbitals [5].

Assuming then that an average of three L-shell vacancies remain when the decay occurs, the $K\alpha^2L^3$ transition has been assigned (though rough agreement is obtained independently [15,24]). This also agrees with the merging of peaks with six or more L-shell vacancies and a corresponding decline in intensity. Low energy $K\beta$ vacancy positions and intensities correspond to tails and asymmetries in the $K\alpha$ peaks, although the $K\beta L^{3,4,5}$ lines have no such confirmation and may be erroneous. In particular the 8.9845 Å peak appears spuriously intense for the assignment given.

It is possible that this intensity may be due to K^2L and $K\beta L^5$ or that the peak is enhanced by the coincidence of the wavelengths of several lines. There is no obvious line unaccounted for and the discrepancy may be due to a fluorescence yield anomaly. Selective electron capture may play a role but this is not reflected in the $K\alpha$ distributions.

A common measure of the ionisation of target atoms is given by the mean L-shell vacancy fraction:

$$p = \sum_n f_n / N,$$

where N is the number of L-shell electrons in the ground state atom and f_n is the fraction of the total X-ray yield contained in the n th multiple-vacancy peak where n is the number of L-shell vacancies [10,12]. Usually the satellites of the peaks shown in the magnesium spectra are not observed, so that each peak is assumed to correspond to a different vacancy number. The present study also assumes that the satellites around each major peak have identical vacancy numbers so that p is calculated by summing all components of each major peak as suggested by the line numbers. The values of p are given in the tables.

The trend to lower L-shell vacancies with higher angles of incidence is dominated by the absorption of the L^{6-7} vacancy lines with the crystal. However, a shift

in the peak intensity from 4 to 3 to 2 L-shell vacancies from spectra 1–3 (due to the angle) is also noted. The reverse effect would be expected from the variation of the incident beam charge state.

The main effect of the differential absorption through the target is to reduce the hypersatellite intensities with respect to the satellites below the absorption edge. This may be estimated from the ratios in the spectra at different angles of incidence. If lines 9–16 are assumed to be purely $K\alpha$ hypersatellite peaks, the ratio $R = I(\text{satellites})/I(\text{hypersatellites})$ may be estimated as 4.68 for the grazing incidence magnesium spectrum and 18.9 for that taken with $\theta = 25^\circ$. The fluorine spectra are incomplete but spectrum 4 provides an overestimate for this ratio of 4.66.

5. A model for intensities

Sputtering or impact at 63 MeV has a sufficiently high cross-section to remain predominantly an interaction of the surface and upper layers of the solid [21]. Electronic recombination is of major importance in solid targets, especially with regard to L-shell vacancy filling by adjacent ions. Nonradiative deexcitation enhances the $K\alpha$ intensity. These processes are not completed before radiative decay occurs and highly-ionised He-like ions may still be produced and observed to decay by X-ray emission.

In order to model the L-shell vacancy intensities the following assumptions are introduced, modified from Endo and Uda [10], who used N^{4+} impact and therefore achieved lower charge state production:

1) The L-shell electrons are ejected simultaneously without correlations between ejected and orbital electrons so that the primary L vacancies are described in terms of the binomial distribution where E is the number of electrons in the shell;

$$y_i = {}_E C_i P^i (1 - P)^{E-i}.$$

This is a simple approximation to the true electron ejection process where correlations may be significant.

2) The L-vacancy rearrangement and recombination probability, dependent upon the KL^n state, can be replaced by an average L-vacancy rearrangement probability f' ;

3) In contrast to Endo and Uda, L-vacancies are produced by the decay of double K vacancies. However, the hypersatellite intensities and L-vacancy production rates follow those of the satellite, so this mechanism is statistically similar to that of 1);

4) Because of the higher initial vacancy production, there is a significant probability of multiple L-shell filling before X-ray emission. Consequently the ob-

served satellite intensity distribution may be given by

$$y_1^0 = A(\omega_1/\omega') (y_1 + f'y_2 + \dots + f'^{E-1}y_E),$$

$$y_n^0 = A(\omega_n/\omega') (1 - f') (y_n + f'y_{n+1} + \dots + f'^{E-n}y_E),$$

where A , ω_n and ω' are the scale factor, the fluorescence yield for the KL^n configuration and the mean fluorescence yield respectively.

5a) Except for fluorine, the ratios ω_n/ω' have been claimed to be approximately unity [22,23].

5b) However, Larkins [25,26] suggested a simple scaling law to generate the neutral atom (by scaling Auger and radiative rates according to the number of electrons available).

5c) This neglects the changing wavefunction as electrons are ejected and does not explicitly take account of closed channels and metastable states [30]. Divergence therefore occurs for few-electron systems. Tawara et al. [27] provide quantum-mechanical derivations of the fluorescence yields and their averages over the configurations for each charge state of fluorine [27], illustrating the difference from yields using Larkin's method. Hopkins et al. [28] provides estimates of Auger and X-ray rates and fluorescence yields for multiply-ionised Al. KLL Auger rates for magnesium are essentially the same as those for aluminium, whereas KLM rates are reduced by 352/617 and X-ray rates are reduced by 425/579 [26]. Neglecting variation of the wavefunction, KMM Auger rates are reduced by 1/3 since magnesium has only two M-shell electrons. This prescription allows fluorescence yields for each configuration to be calculated and averaged for each charge state assuming statistical population of all levels.

These three options provide estimates of the fluorescence yields. The yields for each configuration can vary widely: 0.033:0.083:0.093 for the $1s2s^22p3s^2$: $1s2s2p^23s^2$: $1s2p^33s^2$ configurations of Mg VII [28]. The effective yields are therefore highly dependent upon the assumption of the statistical distribution of populations in levels – and upon the LS-coupling approximation. Comparison of a model assuming the statistical distribution of charge states and two alternative models (for neon) [35] has suggested that the statistical model is appropriate in numerous cases. However, it is known that nonstatistical populations occur for heavier ion impact where few-electron transitions are dominant [3,5]. In particular, Coster–Kronig transitions between sub-levels and selective excitation can modify the calculated yields significantly.

$K\alpha$ -satellite transitions dominate the X-ray emission. There is therefore little error in using total X-ray fluorescence yields rather than $K\alpha$ yields. However, the magnesium estimates using assumption 5c) (above) take account of this difference *neglecting the $K\beta$ enhancement due to selective M-shell electron capture*.

Nonradiative deexcitation and cascading to the single

vacancy state may be modelled by the addition of a coefficient D to the observed $K\alpha$ intensity y_1^0 and a coefficient R_c to the total decay rate. This should be small except for few-electron systems. Thus the $K\alpha$ fluorescence yield is

$$\omega_x = T_x(2p-1s)/(I_x + I_A + R_c)$$

with T_x the $K\alpha$ rate, I_x the total X-ray rate and I_A the sum of the KLL, KLM KMM and other Auger rates. This process does not enhance the hypersatellite K^2L^0 line but depletes particular satellite states preferentially. This latter effect is of secondary importance, especially at low resolution, but the use of a constant rate R_c is of doubtful value. If blocked Auger channels dominate any collision-induced rate, R_c can be negative.

6. Modelling the intensity distributions

Fluorescence yields for these models are given in table 4. Monte Carlo least-squares minimisation of the intensity discrepancies using the above model leads to the values of f' , P , D and the derived calculated intensities from the experimental y_i^0 values as given in table 5.

Note that the fluorine spectra cannot provide good fits due to the poor resolution of the separate peaks and the overlap between lines originating from adjacent charge states in each peak. Significant overlap of the quartet KL^6 state with KL^5 can occur and may be estimated for magnesium and heavier ions [5,35]. However, *most* of the peaks overlap strongly in the fluorine spectra. The results of this overlap is that peaks corresponding to particular *term values* rather than *charge states* tend to group together.

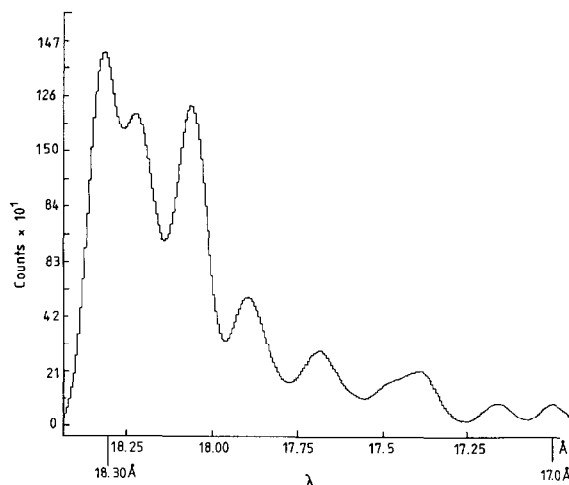


Fig. 6. Fluorine $K\alpha$ multiple-vacancy spectrum calculated assuming statistical populations and using ref. [24] and [27].

Table 4
Fluorescence yields $\times 100$

Model	FII	III	IV	V	VI	VII	VIII	MgII	III	IV	V	VI	VII	VIII	IX
a	ω														
b1	1.41	1.69	2.10	2.78	4.11	7.90	100.	3.43	3.96	4.69	5.74	7.39	10.4	17.5	54.7
b2	1.41	1.68	2.09	2.76	4.07	7.68	58.8	3.42	3.95	4.66	5.69	7.29	10.1	16.3	38.1
c1	1.23	1.40	1.74	2.68	7.13	19.2	55.4	3.07	3.34	3.70	4.37	5.24	6.90	10.7	28.1
c2								3.06	3.32	3.67	4.33	5.16	6.72	10.1	21.0

Models a, b, c are described under assumption 5 in the text. b1, c1 assume no nonradiative transition other than the Auger rates; b2, c2 assume $R_c = 0.1$, $0.15 \times T_x(K_\alpha L^0)$ independent of the ionisation state.

Calculation of theoretical spectra using all LS terms can quantify and allow for this overlap. Fig. 6 shows an approximate fit using theoretical wavelengths and fluorescence yields. The discrepancies between the theoretical and experimental positions are clear, suggesting that even experiments of this resolution can yield better values for the peak wavelengths than calculated spectra. The discrepancy between the fitted peak intensities and the intensities of each charge state for fluorine is also clear from table 5.

Another problem arises from the background level. Use of a "local" fitted background involving adjacent peaks can lead to accurate wavelengths while providing distorted intensities. Approximate correction for this has been made for the magnesium spectra.

In the derivation of accurate P and f' values all spectra (but especially high-angle spectra) should be corrected for absorption. Although it is this variation with angle which exposes the advantage of the grazing-incidence technique, it is useful to attempt to compare the excitation and deexcitation conditions of the recoils in each geometry. In achieving this, a formalism modified from that of Watson et al. [12,31] for the different geometry was adopted. However, the possibility of recoil ion motion (normal to the beam) prior to emission is also considered.

Ranges of ions were estimated from ref. [21] and absorption corrections were applied using the empirical law $\mu = C\lambda^n$ for each side of the K-edge [33]. The relation was fitted to the data of reference [34] to correct the intensities for each channel, allowing the peaks to be (re-)fitted after this. Correction for detector window absorption was also made.

The estimated ion range was $25.4 \mu\text{m}$, of which highly-ionized transitions are excited within the first $5\text{--}10 \mu\text{m}$. The binary encounter approximation suggests that at high velocities the cross-section for ionization is roughly constant. After charge equilibrium is attained in the beam, further slowing of the target reduces the mean charge state and lowers the probability of multiple-vacancy production [36,37]. Assuming uniform excitation to the depth of $5 \mu\text{m}$ provided a reasonable correction. An estimate of the typical recoil energy and excited state lifetime provided a negligible recoil correction to this absorption.

The results of the fits of intensities with the models used are given in table 5 and fig. 7 shows one example graphically. Note that D is significant in all spectra except for the hypersatellite fitting, as expected. Although D may therefore be an appropriate parameter (that is, a parameter modelling an important and significant physical process), f' is usually 0.0, suggesting that no L-shell electron capture occurs before deexcitation. This is not true of the $K\beta$ hypersatellite intensities, and the physical value of $f' = 0.17$ may be appropriate in these highly-excited states. With the consid-

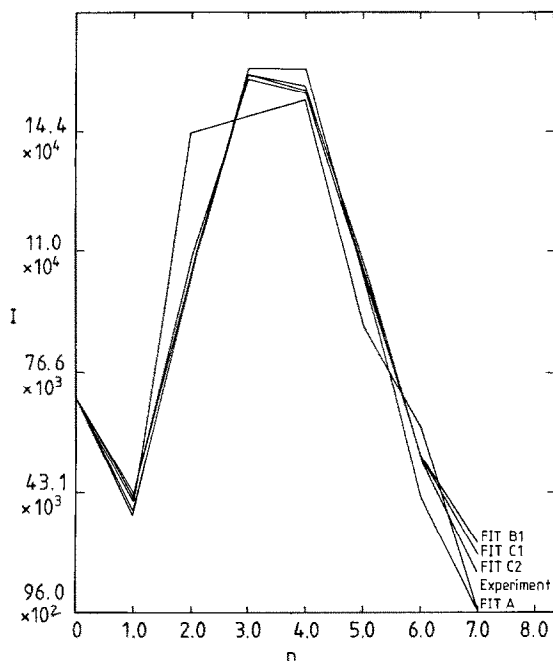


Fig. 7. Fitted intensities (in counts summed over channels) for the Mg multiple-vacancy peaks of spectrum 1. n is the number of initial L-shell vacancies.

erable fitting errors involved in extracting intensities and the close negative correlation between P and f' , the value of f' obtained should be treated with caution.

$f' = 0.0$ in the other fits because the third (KL^2) peak has a consistently high intensity. This is due to overlap of lines arising from adjacent charge states and is responsible for the poor fits. Correction for overlap is possible assuming statistical distribution of states, the term wavelengths, but this has only been attempted in the case of fluorine [24].

The models using more carefully derived values for the fluorescence yields were generally no better than those assuming uniform yields. This is due to the difficulty of deriving accurate intensities from the data and uncorrected overlap, as seen in the fluorine spectra.

The binomial excitation probability P varied from 0.34 to 0.44. The model-dependent variation was greater than the variation between spectra 1–3, although the probability was highest for the spectrum taken at grazing incidence.

7. Conclusion

Solid target observation at medium resolution and grazing incidence has been shown to provide well-defined multiple-vacancy peaks with greater intensities of higher charge states than previously observed. Estimated calibration to $\pm 0.005 \text{ \AA}$ allowed identification of

the K and L-shell configuration but yielded uncertainty with respect to the number of M-shell electrons and the term values. Statistical averages-over-configurations for calculated wavelengths provide reasonable correspondence to the fitted values, but the errors of roughly $\pm 0.01 \text{ \AA}$ in these values prevent identification of the nonstatistical nature of the excitation and the M-shell occupation.

The large ratio of $K\beta$ to $K\alpha$ hypersatellites in spectrum 1 suggests that selective electron recombination to the M-shell occurs from adjacent ions in the solid before radiative deexcitation. A model for the excitation process is combined with various estimates for the fluorescence yields and a Monte Carlo fitting of relative intensities. The use of averages-of-configuration and assumptions of a statistical distribution allow reasonable fits to the experimental intensities after correction for background and absorption effects. The model uses a binomial excitation probability for L-shell vacancy production P , an average L-vacancy rearrangement probability f' and a nonradiative deexcitation and cascading rate D . f' and P have a close negative correlation so that errors in the data may distort the fitted values for these parameters. The modelling leads to the value of P between 0.34 and 0.44. The model-dependent variation was greater than the variation between spectra, although P was greatest for the spectrum taken at grazing incidence.

The major advantage of the grazing-incidence technique lies in the limitation of the excitation to the surface layers of the solid and the consequent reduction of the absorption effects.

Comparison of theoretical wavelengths to spectra 1 and 4/5 suggests that the wavelengths of satellites to helium-like lines may be measured to reasonable precision. Higher resolution will resolve any M-shell occupation and may reveal hydrogenic and helium-like transitions perturbed only by weakly-bound highly-excited electrons. This implies that the intention to test QED using solid targets may be feasible with high-resolution spectroscopy. Higher charge state impact using higher charge, heavy-ion accelerators may be required to yield a sufficient intensity of highly-ionised recoils in solids for precision Lamb shift measurements.

Acknowledgement is made to J.M. Laming and A.F. McClelland for assistance and discussions, and to R. MacDonald for assistance during one of the runs. One of us (C.C.) is sponsored by Shell Australia for this work.

References

- [1] R. Mann et al., Phys. Rev. Lett. 46 (1981) 646.
- [2] R. Mann et al., J. Phys. B14 (1981) 1161.
- [3] H.A. Klein et al., J. Phys. B15 (1982) 4507.

- [4] J.A. Demarest and R.L. Watson, *Phys. Rev.* A17 (1978) 1302.
- [5] R.L. Kauffman et al., *Phys. Rev.* A11 (1975) 872.
- [6] F. Folkmann et al., *Phys. Scripta* 73 (1983) 88.
- [7] F. Folkmann et al., *Nucl. Instr. and Meth.* 181 (1981) 99.
- [8] I.A. Armour et al., *J. Phys.* B15 (1980) 2701.
- [9] E. Träbert et al., *J. Phys.* B15 (1982) 3587.
- [10] H. Endo and M. Uda, *Z. Phys.* A306 (1982) 187.
- [11] S. Datz, *Phys. Scripta* T3 (1983) 79.
- [12] R.L. Watson et al., *Phys. Rev.* A15 (1977) 914.
- [13] O. Benka et al., *Phys. Rev. Lett* 47 (1981) 1202.
- [14] C.F. Moore et al., *Phys. Lett.* 54A (1975) 407.
- [15] R.L. Watson et al., *Phys. Scripta* 31 (1985) 184.
- [16] J.S. Bashkin and J.O. Stoner Jr., *Atomic Energy Levels and Grotrian Diagrams*, (North-Holland, Amsterdam, 1971).
- [17] *CRC Handbook of Chemistry and Physics*, ed. R.C. Weast, 60th ed. (CRC Press, Florida, 1980).
- [18] A.M. Ermolaev and M. Jones, *J. Phys.* B7 (1974) 199.
- [19] A. Russek, *Phys. Rev.* 132 (1963) 246.
- [20] H.F. Beyer et al., *J. Phys.* B13 (1980) 2459.
- [21] L.C. Northcliffe and R.F. Schilling, *Nucl. Data Tables* A7 (1970) 233.
- [22] V. Dutkiewicz, H. Bakhra and N. Cue, *Phys. Rev.* A13 (1976) 306.
- [23] J.A. Tanis et al., *Phys. Rev.* A20 (1979) 2440.
- [24] R.J. Maurer and R.L. Watson, *At. Data and Nucl. Data Tables* 34 (1986) 185.
- [25] F.P. Larkins, *J. Phys.* B4 (1971) L29.
- [26] E.J. McGuire, *Phys. Rev.* A2 (1970) 273.
- [27] H. Tawara, P. Richard et al., *Phys. Rev.* A19 (1979) 1960.
- [28] F. Hopkins et al., *Phys. Rev.* A8 (1973) 2952.
- [29] J.S. Hanson et al., *Nucl. Phys.* A142 (1970) 604.
- [30] C.P. Bhalla et al., *Phys. Rev.* A8 (1973) 649.
- [31] R.L. Watson et al., *Phys. Rev.* A10 (1974) 1230.
- [32] W. Bambynek et al., *Rev. Mod. Phys.* 44 (1972) 716, *Rev. Mod. Phys.* 46 (1974) 853.
- [33] G.L. Clark, *The Encyclopedia of X-rays and gamma rays*. (Reinhold Publishing Co., 1963).
- [34] B.L. Henke et al., *At. Data Nucl. Data Tables* 27 (1982) 1.
- [35] M.H. Chen and B. Crasemann, *Phys. Rev.* A12 (1975) 959.
- [36] H-D. Betz, *Rev. Mod. Phys.* 44 (1972) 465.
- [37] J.H. McGuire and P. Richard, *Phys. Rev.* A8 (1973) 1374.
- [38] L.A. Vainshtein and U.I. Safranova, *At. Data Nucl. Data Tables* 21 (1978) 49.